

Adaptive Output Feedback Control for 5-DOF Varying-Cable-Length Tower Cranes With Cargo Mass Estimation

Yiming Wu, Ning Sun, *Senior Member, IEEE*, He Chen, *Member, IEEE*, and Yongchun Fang, *Senior Member, IEEE*

Abstract—Tower crane systems exhibit high nonlinearity and underactuation, making the control issue challenging. Most reported methods for tower crane systems utilize linearized models, and accurate plant parameters (e.g., cargo mass, jib moment inertia) and full state feedback are usually required; moreover, most existing works only consider a part of the crane motions, and the control issue of 5 degree-of-freedom (5-DOF) tower cranes (i.e., 2-DOF cargo swing, slew, hoisting, and translation) is still open. However, tower cranes are practically influenced by uncertainties and disturbances, which may make linearized models ineffective; additionally, exact values of plant parameters may be difficult to obtain, and velocity signals are usually not directly measurable in practice. To address the aforementioned problems, this paper proposes an adaptive output feedback control method for 5-DOF varying-cable-length tower cranes. As far as we know, the paper provides the first adaptive output feedback controller, designed and analyzed without linearizing the dynamic equations, which can simultaneously achieve cargo hoisting/lowering, jib slew, trolley translation, and swing suppression, by avoiding using velocity-related feedback signals. Resorting to an elaborately constructed virtual spring-mass system, the control objectives are satisfactorily achieved even without involving any velocity signals with theoretical/experimental guarantee. Moreover, by elaborately designing a new adaptive law, the exact values of unknown cargo masses can be estimated through online identification. We provide rigorous stability/convergence analysis for the closed-loop system. Hardware experiment results are included for effectiveness/robustness verification.

Index Terms—Mechatronics, motion control, tower cranes, varying cable length.

I. INTRODUCTION

CRAINE systems are widely utilized to transport heavy and huge cargoes, which play important roles in various fields of modern industry. For example, overhead cranes equipped like bridges are utilized to transport materials in workshops, offshore cranes are set upon ships to load/upload cargoes on the sea, and tower cranes are an important kind of mechatronic equipment in construction sites. These crane systems are special kinds of underactuated systems with low costs and simple mechanical structure. For mechatronic or robotic systems, such as flying robots [1], mobile vehicles [2], [3], manipulators [4], [5], and many other nonlinear systems [6], [7], there have been

This work was supported in part by the National Natural Science Foundation of China under Grant 61873134 and Grant U1706228, in part by the Young Elite Scientists Sponsorship Program by Tianjin under Grant TJSQNTJ-2017-02, and in part by the Tianjin Research Innovation Project for Postgraduate Students under Grant 2019YJSB070. (*Corresponding author: Ning Sun*.)

Y. Wu, N. Sun, and Y. Fang are with the Institute of Robotics and Automatic Information Systems, College of Artificial Intelligence, and also with the Tianjin Key Laboratory of Intelligent Robotics, Nankai University, Tianjin 300350, China (e-mail: sunn@nankai.edu.cn).

H. Chen is with the School of Artificial Intelligence, Hebei University of Technology, Tianjin, China 300401.

abundant meaningful control methods reported. Nevertheless, different from those systems, for cranes, the unactuated cargo swings cannot be directly controlled, which bring difficulties and challenges for control development.

This paper studies the control issue of underactuated tower crane systems with cargo hoisting/lowering motions. As for the mechanical structure, a tower crane system has a long mast fixed on a base to make it high enough to reach tall buildings, a jib rotating around the mast, and a trolley moving along the jib. Cargoes are suspended beneath the trolley by steel cables, whose lengths can be adjusted/controlled to complete hoisting/lowering tasks. During transportation, the cargo swings are coupled with the jib slew motion, trolley translation, and also cable length variation, which produce very complicated dynamic coupling and make the control problem very challenging.

A. Research Background of Cranes

Presently, for different kinds of cranes (including overhead cranes, offshore cranes, boom cranes, etc.), a lot of efforts have been made. Specifically, input shaping techniques and trajectory/path planners are studied in [8]–[11]. In [8], a frequency-modulation input shaping technique is developed to eliminate resonant frequencies. In [9], a non-time based regulator is presented for path tracking control. Considering different aspects, optimal paths are generated for dual-crane systems in [10], which also achieves collision avoidance and cooperative works. In [11], a trajectory tracking controller is presented together with feedforward control design to reduce steady errors. Apart from open-loop planners, in order to enhance robustness, many feedback controllers are also developed, including sliding mode control [12], [13], fuzzy control [14]–[17], and neural network control [18]. Specifically, Ngo *et al.* apply sliding mode techniques to control the lateral sway motion of an offshore crane [12]. The sliding mode technique is also used together with the backstepping control method to achieve anti-swing trajectory tracking of 3D overhead cranes [13]. As for fuzzy control, the control parameters can be tuned by the designed adaptive algorithm in [14]; the fuzzy system is utilized as a control gain tuner in [15]; a genetic algorithm is applied to tune the fuzzy controller's parameters in [16]; a fuzzy logic-based controller is proposed to achieve anti-swing control without measuring cargo swing angles in [17]. Moreover, an updating rule for neural networks is presented with online learning stability in [18]. There also exist many other anti-swing methods designed for crane systems, such as energy-based control [19], partial feedback linearized control method [20], and H-infinity control [21], [22]. Moreover,

more complicated characteristics of cranes are investigated, for example, distributed-mass cargo in [23] and double-pendulum effects in [24].

However, although the working principles are similar among different kinds of cranes, tower cranes exhibit special characteristics, due to suffering from *strong* underactuation and *severe* disturbances as they are mostly applied under unfavourable aerial working environments. As a result, tower cranes exhibit *complicated* characteristics, and most of the aforementioned methods for other kinds of cranes *cannot* be directly applied to tower cranes. Until now, although tower cranes are widely applied in practice, the control issue is still open with few existing results [25]–[31]. Specifically, a command-shaping algorithm is designed for fixed-cable-length tower cranes to suppress cargo swings in [25], which is an open-loop method and is sensitive to uncertainties. In [26], a model predictive controller is adopted to solve the path-following issue of tower cranes, which is discrete. Further, without path planning, in [27], the suggested feedback controller achieves point-to-point cargo transportation, which ensures one-cycle residual swings. Also, considering practical efficiency problems, in [28], a time-optimal velocity controller is presented by using Pontryagin's maximum principle, which is only based on the cargo dynamics. With more concerns on robustness, in [29], an adaptive method is proposed cooperated with sliding mode-based control to ensure robustness. Moreover, a recurrent neural network controller together with swarm optimization and genetic algorithms is presented in [30]. Different system structures also have influence on control performance. For example, in [31], tower cranes with two hoisting cables are investigated.

B. Motivation and Contribution

Among the limited amount of the existing control methods for tower cranes, there still exist some to-be-addressed issues: (1) Most existing methods cannot simultaneously control cargo hoisting/lowering, jib slew, and trolley translation motions of 5-DOF tower cranes. (2) For most control methods, plant parameters are needed, while in some situations, exact values of plant parameters are difficult to derive; for instance, cargo masses vary in different tasks, and if their accurate values are unavailable, vertical positioning errors will definitely appear for those methods that need exact plant parameters, due to imperfect gravity compensation. (3) In practice, velocity signals are usually difficult to measure and are usually generated by numerical differentiation instead, which may induce noises and degrade the control performance or even bring damage to actuators. (4) Most methods utilize *linearized* models by making small angle assumptions near the equilibrium point. In some situations, cargoes may be disturbed severely and swing far away from the equilibrium point, making simplified models invalid.

To tackle these problems, this paper proposes a nonlinear adaptive output feedback control method for 5-DOF varying-cable-length tower cranes, which can complete cargo transportation tasks and also identify unknown cargo masses accurately. The main contribution can be summarized as follows

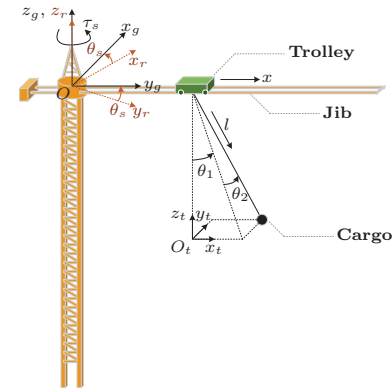


Fig. 1. Model of 5-DOF varying-cable-length tower cranes.

(the following points are summarized after comparing the proposed method with existing related works, and they correspond to the detailed controller designs/analysis, experiments, etc., in the subsequent sections):

- 1) This paper provides a nonlinear controller for underactuated 5-DOF tower cranes, which is the *first adaptive output feedback* method, developed/analyzed *without* linearizing the nonlinear dynamics, which can achieve cargo hoisting/lowering, jib slew, trolley transportation, and swing suppression, simultaneously, by making use of *only* position/angle measurement. The closed-loop system's equilibrium point is proven to be asymptotically stable with rigorous stability analysis.
- 2) The proposed controller needs no plant parameters and hence is insensitive to parameter changes/uncertainties. Moreover, by elaborately designing an adaptive law, the exact values of unknown cargo masses can be derived through online identification. It is noted that, for existing model-based adaptive gravity compensation methods, some complicated gain conditions (inequalities) are usually needed to ensure asymptotic stability; by contrast, no such restrictions are needed for the proposed method, which is a practical merit.
- 3) The proposed controller *avoids* using velocity-related feedback signals, which are replaced by an elaborately constructed virtual spring-mass system. By doing so, there is no need to equip velocity sensors and the troubles caused by numerical differentiation-induced noises are avoided, which is another practical advantage.

The rest of the paper is organized as follows: Section II provides the dynamic model of varying-cable-length tower crane systems and also formulates the control problem. Based on the model, the detailed control design and stability analysis are given in Section III. Then, Section IV verifies the effectiveness of the proposed controller by hardware experiments. Finally, Section V summarizes the entire paper.

II. PROBLEM FORMULATION

The tower crane model is illustrated in Fig. 1, and the dynamic equations can be obtained based on Lagrange's modeling technique [27], the expressions of which are given

TABLE I
PARAMETERS AND VARIABLES

Symbols	Parameters/Variables	Units
m_c, m_t	cargo and trolley masses	kg
J	jib moment inertia	kg·m ²
$\theta_s(t)$	jib slew angle	rad
$x(t)$	trolley translation displacement	m
$l(t)$	varying cable length	m
$\theta_1(t), \theta_2(t)$	cargo radial and tangential swing angles	rad
$\tau_s(t)$	resultant torque controlling jib slew	N·m
$F_x(t)$	resultant force controlling trolley translation	N
$F_l(t)$	resultant force controlling cable length	N
g	gravitational coefficient	m/s ²

in Appendix A for brevity, and the corresponding compact matrix-vector form are given as follows:

$$M(\mathbf{q})\ddot{\mathbf{q}} + C(\mathbf{q}, \dot{\mathbf{q}})\dot{\mathbf{q}} + G(\mathbf{q}) = \mathbf{U}. \quad (1)$$

In (1), $\mathbf{q} = [\theta_s, x, l, \theta_1, \theta_2]^\top$ denotes the state vector, $\mathbf{U} = [\tau_s, F_x, F_l, 0, 0]^\top$ denotes the control input vector, $M(\mathbf{q})$, $C(\mathbf{q}, \dot{\mathbf{q}})$ are the inertia matrix and the centripetal-Coriolis matrix, and $G(\mathbf{q})$ is the gravitational vector. The definitions of $M(\mathbf{q})$, $C(\mathbf{q}, \dot{\mathbf{q}})$, $G(\mathbf{q})$ are given in Appendix B. The state variables and parameters are defined in TABLE I; moreover, $\tau_s \triangleq \tau_{sa} - \tau_{sf}$, $F_x \triangleq F_{xa} - F_{xf}$, $F_l \triangleq F_{la} - F_{lf}$, with τ_{sa} , F_{xa} , F_{la} being the torque/forces directly actuated by motors and τ_{sf} , F_{xf} , F_{lf} being frictions which will be addressed through feedforward compensation in experiments. Particularly, in Fig. 1, along with the jib slew motion, the jib-fixed coordinate $\{O - x_r y_r z_r\}$ rotates around the z_r -axis and becomes $\{O - x_g y_g z_g\}$; also, $\{O_t - x_t y_t z_t\}$ denotes the trolley-coordinate.

As commonly done in the crane control-related literature [8]–[31], the following assumption is made by considering practical application situations:

Assumption 1: The cable is rigid. The mass and density of the cable are ignored. The cargoes are beneath the jib, that is, the swing angles satisfy $-\pi/2 < \theta_1(t), \theta_2(t) < \pi/2$.

In this paper, for 5-DOF tower crane systems with *unknown* plant parameters, it is needed to design an adaptive output feedback controller (*without* using velocity signals) for $\tau_s(t)$, $F_x(t)$, $F_l(t)$ to achieve the following objectives, *without* linearizing the complicated dynamics:

- Achieve accurate positioning control by controlling the jib slew angle $\theta_s(t)$, the trolley translation displacement $x(t)$, and the suspension cable length $l(t)$ to their desired values θ_{sd} , x_d , l_d , respectively, in the sense that

$$\theta_s(t) \rightarrow \theta_{sd}, \quad x(t) \rightarrow x_d, \quad l(t) \rightarrow l_d. \quad (2)$$

- Suppress unactuated cargo swings, in the sense that

$$\theta_1(t) \rightarrow 0, \quad \theta_2(t) \rightarrow 0. \quad (3)$$

- Estimate unknown cargo masses accurately, i.e.,

$$\tilde{m}_c \rightarrow 0, \quad (4)$$

where $\tilde{m}_c \triangleq m_c - \hat{m}_c$, with \hat{m}_c , \tilde{m}_c being the estimation and the estimation error of m_c , respectively.

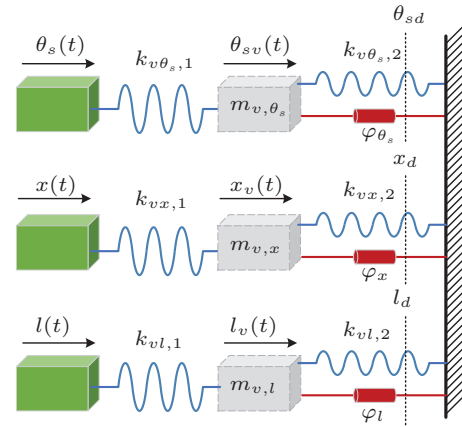


Fig. 2. Illustration of the constructed virtual spring-mass system.

- Restrict the suspension cable length within the range of (l_m, l_M) , where $l_m, l_M \in \mathbb{R}^+$ are the lower and upper bounds of the varying cable length, respectively.

III. MAIN RESULTS

The section will detail both the adaptive output feedback controller design and the corresponding stability/convergence analysis.

A. Output Feedback Controller Design

In practice, most cranes are not equipped with velocity sensors; hence, to meet the requirements of state feedback controllers, velocities are alternatively obtained by numerical differentiation, which may easily induce unexpected noises and degrade the control performance. In this paper, in order to avoid using velocity signals, we introduce a virtual spring-mass system to describe the relationship between the actuated state variables and their desired positions, which will be utilized in the subsequent output feedback controller design and stability analysis. To this end, the virtual spring-mass system is designed as follows:

$$\begin{aligned} m_{v,\theta_s} \ddot{\theta}_{sv} &= -k_{v\theta_s,1}(\theta_{sv} - \theta_s) + k_{v\theta_s,2}(\theta_{sd} - \theta_{sv}) - \varphi_{\theta_s} \dot{\theta}_{sv}, \\ m_{v,x} \ddot{x}_v &= -k_{vx,1}(x_v - x) + k_{vx,2}(x_d - x_v) - \varphi_x \dot{x}_v, \\ m_{v,l} \ddot{l}_v &= -k_{vl,1}(l_v - l) + k_{vl,2}(l_d - l_v) - \varphi_l \dot{l}_v, \end{aligned} \quad (5)$$

where m_{v,θ_s} , $m_{v,x}$, $m_{v,l}$ denote the virtual masses, $k_{v\theta_s,1}$, $k_{v\theta_s,2}$, $k_{vx,1}$, $k_{vx,2}$, $k_{vl,1}$, $k_{vl,2}$ denote the stiffness coefficients of virtual springs, φ_{θ_s} , φ_x , φ_l denote the virtual damping coefficients, and $\theta_{sv}(t)$, $x_v(t)$, $l_v(t)$ denote the virtual displacements of the virtual masses, respectively. The introduced system (5) is essentially a second-order filter, which is introduced independently of the tower crane system and will be utilized to complete the subsequent stability analysis. To make its physical significance more intuitive, a schematic illustration is given in Fig. 2. Subsequently, the introduced virtual system will be utilized to design an output feedback controller without using velocity signals.

In order to implement the system in subsequent controller design without measuring the velocity signals, the three subsystems in (5) are alternatively realized through the following

equations, respectively, to dynamically generate the virtual signals $\theta_{sv}(t)$, $x_v(t)$, $l_v(t)$:

$$\begin{aligned}\dot{\theta}_{sv} &= \frac{1}{m_{v,\theta_s}}(\xi_{\theta_{sv}} - \varphi_{\theta_s}\theta_{sv}), \\ \dot{\xi}_{\theta_{sv}} &= -(k_{v\theta_{s,1}} + k_{v\theta_{s,2}})\theta_{sv} + k_{v\theta_{s,1}}\theta_s + k_{v\theta_{s,2}}\theta_{sd}, \\ \dot{x}_v &= \frac{1}{m_{v,x}}(\xi_x - \varphi_x x_v), \\ \dot{\xi}_x &= -(k_{vx,1} + k_{vx,2})x_v + k_{vx,1}x + k_{vx,2}x_d, \\ \dot{l}_v &= \frac{1}{m_{v,l}}(\xi_l - \varphi_l l_v), \\ \dot{\xi}_l &= -(k_{vl,1} + k_{vl,2})l_v + k_{vl,1}l + k_{vl,2}l_d, \end{aligned}\quad (6)$$

where $\xi_{\theta_s}(t)$, $\xi_x(t)$, $\xi_l(t)$ are constructed auxiliary filter variables¹ and one has $\xi_i(0) = 0$, $i = \theta_s$, x , l , and $\theta_{sv}(0) = 0$, $x_v(0) = 0$, $l_v(0) = l(0)$.

The energy of the entire virtual system is depicted in the following manner:

$$E_v = \frac{1}{2} \left[m_{v,\theta_s} \dot{\theta}_{sv}^2 + m_{v,x} \dot{x}_v^2 + m_{v,l} \dot{l}_v^2 + k_{v\theta_{s,1}} (\theta_{sv} - \theta_s)^2 + k_{v\theta_{s,2}} (\theta_{sd} - \theta_{sv})^2 + k_{vl,1} (l_v - l)^2 + k_{vl,2} (l_d - l_v)^2 + k_{vx,1} (x_v - x)^2 + k_{vx,2} (x_d - x_v)^2 \right]. \quad (7)$$

By using $E_v(t)$ in (7) and defining $\dot{q}(t) = [\dot{\theta}_s(t), \dot{x}(t), \dot{l}(t), \dot{\theta}_1(t), \dot{\theta}_2(t)]^\top$, the following energy-like function $E(t)$ can be obtained:

$$E = \frac{1}{2} \dot{q}^\top M \dot{q} + m_c g l (1 - \cos \theta_1 \cos \theta_2) + E_v. \quad (8)$$

Then, by differentiating $E(t)$ and using (50)–(54), (5), and (7), one has that

$$\begin{aligned}\dot{E} &= \tau_s \dot{\theta}_s + F_x \dot{x} + (F_l + m_c g) \dot{l} + \dot{E}_v \\ &= [\tau_s - k_{v\theta_{s,1}} (\theta_{sv} - \theta_s)] \dot{\theta}_s + [F_x - k_{vx,1} (x_v - x)] \dot{x} \\ &\quad + [F_l + m_c g - k_{vl,1} (l_v - l)] \dot{l} \\ &\quad - \varphi_{\theta_s} \dot{\theta}_{sv}^2 - \varphi_x \dot{x}_v^2 - \varphi_l \dot{l}_v^2.\end{aligned}\quad (9)$$

On the basis of (8), (9), and the subsequent analysis, the following adaptive output feedback controller is designed:

$$\tau_s = -k_{p1} e_{\theta_s} + k_{v\theta_{s,1}} (\theta_{sv} - \theta_s), \quad (10)$$

$$F_x = -k_{p2} e_x + k_{vx,1} (x_v - x), \quad (11)$$

$$F_l = -k_{p3} e_l - y(l) + k_{vl,1} (l_v - l) - \hat{m}_c g, \quad (12)$$

where $e_{\theta_s}(t)$, $e_x(t)$, $e_l(t)$ are error signals defined as follows:

$$e_{\theta_s} = \theta_s - \theta_{sd}, \quad e_x = x - x_d, \quad e_l = l - l_d, \quad (13)$$

and $\theta_{sv}(t)$, $x_v(t)$, $l_v(t)$ are dynamically generated by (6) without using velocity measurements, through only integrating operations without numerical differentiating; k_l , k_{pi} 's $\in \mathbb{R}^+$, $i = 1, 2, 3$ are control gains; \hat{m}_c indicates the mass estimation defined as follows:

$$\hat{m}_c \triangleq \hat{m}_{cp} + \hat{m}_{cs},$$

¹ $\xi_{\theta_{sv}}(t)$, $\xi_x(t)$, $\xi_l(t)$, which are introduced for notation brevity, are three intermediate variables that are not actually used in the ultimate controller. They can be generated from (6) by integrating operations (without any numerical differentiating operations).

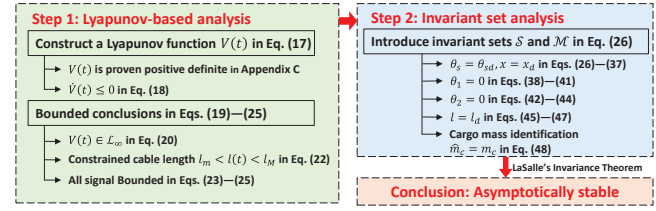


Fig. 3. The block diagram of the entire stability analysis.

where \hat{m}_{cp} , \hat{m}_{cs} denote the preliminary and supplementary mass estimations, respectively. In order to achieve gravitational compensation, an adaptive updating law of \hat{m}_{cp} is presented together with the design of \hat{m}_{cs} , which are given respectively as follows:

$$\dot{\hat{m}}_{cp} = \frac{g \dot{l}}{k_{m1}}, \quad \hat{m}_{cs}(e_l) = k_{m2} \cdot \frac{\left[\int_0^t e_l(\rho) d\rho \right]^2}{1 + \left[\int_0^t e_l(\rho) d\rho \right]^2} \cdot e_l, \quad (14)$$

where k_{m1} , $k_{m2} \in \mathbb{R}^+$ are to-be-determined coefficients. Then one has $\hat{m}_c = \frac{g}{k_{m1}}[l - l(0)] + k_{m2} \cdot \frac{\left[\int_0^t e_l(\rho) d\rho \right]^2}{1 + \left[\int_0^t e_l(\rho) d\rho \right]^2} \cdot e_l$.

Also, in (12), we design

$$y(l) = -k_l \frac{\frac{\arctan(l_M - l)}{1 + (l - l_m)^2} - \frac{\arctan(l - l_m)}{1 + (l_M - l)^2}}{\arctan^2(l - l_m) \arctan^2(l_M - l)} \cdot e_l^2 + \frac{2k_l e_l}{\arctan(l - l_m) \arctan(l_M - l)}. \quad (15)$$

Moreover, the cable always has a non-zero initial length $l(0)$ in practice, which satisfies $0 < l_m < l(0) < l_M$, so as to leave adjustable space between the trolley and cargo, and prevent collision.

Then, by applying the proposed control law and the mass estimations in (10)–(14), the equilibrium point of the closed-loop system can be proven to be asymptotically stable with rigorous theoretical analysis.

Remark 1: Unknown cargo mass can be compensated by the two parts in (14), which are designed through reverse deduction and are closely related to the subsequent stability analysis process. Briefly speaking, by designing (14), together with the proposed controller (10)–(12), one can make the Lyapunov function candidate's time derivative (18) be nonpositive, to further deduce asymptotically stable results.

B. Stability Analysis

Before providing theoretical analysis, the following lemma is given first:

Lemma 1: LaSalle's Invariance Theorem [32]: Given a representation of the system $\dot{x} = f(x)$, where x is the vector of variables with $f(0) = 0$. If a C^1 function $V(x)$ can be found such that $V(x)$ is positive definite and $\dot{V}(x)$ is negative semi-definite, i.e., $V(x) > 0$, $\forall x \neq 0$, $V(0) = 0$, $\dot{V}(x) \leq 0$, $\forall x$, and also if the largest invariant set \mathcal{I} contained in the set $\{x : \dot{V}(x) = 0\}$ contains only the system equilibrium point, then the system is asymptotically stable.

Theorem 1: For the tower crane dynamics given in (50)–(54), the proposed controller in (10)–(12) guarantees that, when $t \rightarrow \infty$,

- The positioning errors asymptotically converge to zero, i.e.,

$$\begin{aligned} e_{\theta_s} &\rightarrow 0, \quad e_x \rightarrow 0, \quad e_l \rightarrow 0, \quad \theta_1 \rightarrow 0, \quad \theta_2 \rightarrow 0, \\ \dot{e}_{\theta_s} &\rightarrow 0, \quad \dot{e}_x \rightarrow 0, \quad \dot{e}_l \rightarrow 0, \quad \dot{\theta}_1 \rightarrow 0, \quad \dot{\theta}_2 \rightarrow 0. \end{aligned} \quad (16)$$

- The unknown cargo mass estimation error \tilde{m}_c asymptotically converge to zero, i.e., $\tilde{m}_c \rightarrow 0$.

- The cable length $l(t)$ satisfies that $0 < l_m < l < l_M$.

Proof: To be clear, the proof of *Theorem 1* will be proceeded step by step (2 steps in total) as summarized in Fig. 3.

Step 1: It will be proven consequently that the state variables are bounded. By using (8), the following energy-like function $V(t)$ is constructed (which is proven to be positive definite on $l(t) > 0$ in Appendix C):

$$\begin{aligned} V = & \frac{1}{2} \dot{\mathbf{q}}^\top M \dot{\mathbf{q}} + m_c g l (1 - \cos \theta_1 \cos \theta_2) \\ & + \frac{1}{2} k_{p1} e_{\theta_s}^2 + \frac{1}{2} k_{p2} e_x^2 + \frac{1}{2} k_{p3} e_l^2 + \frac{1}{2} k_{m1} \tilde{m}_c^2 \\ & + g \int_0^{e_l} \hat{m}_{cs}(\tau) d\tau + \frac{k_l e_l^2}{\arctan(l - l_m) \arctan(l_M - l)} \\ & + \frac{1}{2} [m_{v,\theta_s} \dot{\theta}_{sv}^2 + m_{v,x} \dot{x}_v^2 + m_{v,l} \dot{l}_v^2 + k_{v\theta_{s,1}} (\theta_{sv} - \theta_s)^2 \\ & + k_{v\theta_{s,2}} (\theta_{sd} - \theta_{sv})^2 + k_{vl,1} (l_v - l)^2 + k_{vl,2} (l_d - l_v)^2 \\ & + k_{vx,1} (x_v - x)^2 + k_{vx,2} (x_d - x_v)^2], \end{aligned} \quad (17)$$

where $\tilde{m}_{cp} \triangleq m_c - \hat{m}_{cp}$. Taking the time derivative of (17) and inserting (9)–(14), one can obtain that

$$\begin{aligned} \dot{V} = & \dot{\theta}_s [\tau_s + k_{p1} e_s - k_{v\theta_{s,1}} (\theta_{sv} - \theta_s)] + \dot{x} [F_x + k_{p2} e_x \\ & - k_{vx,1} (x_v - x)] + \dot{l} [F_l + m_c g + y(l) \\ & + \hat{m}_{cs} g + k_{p3} e_l - k_{vl,1} (l_v - l)] \\ & + k_{m1} \tilde{m}_{cp} \dot{\tilde{m}}_{cp} - \varphi_{\theta_s} \dot{\theta}_{sv}^2 - \varphi_x \dot{x}_v^2 - \varphi_l \dot{l}_v^2 \\ = & - \varphi_{\theta_s} \dot{\theta}_{sv}^2 - \varphi_x \dot{x}_v^2 - \varphi_l \dot{l}_v^2, \end{aligned} \quad (18)$$

which indicates that $\dot{V}(t)$ is nonpositive and the following conclusion can be obtained:

$$V(t) \leq V(0). \quad (19)$$

Then, by setting $0 < l_m \leq l(0) \leq l_M$, it can be concluded from (17) that

$$0 \leq V(0) \leq +\infty \implies V(t) \leq V(0) \leq +\infty. \quad (20)$$

Subsequently, we will prove that the cable length $l(t)$ always varies within the given range (l_m, l_M). Assuming that $l(t)$ tends to escape the given range, since $l_m < l(0) < l_M$, there at least exists one $t' \in (0, +\infty)$ such that $l(t') \rightarrow l_m^+$ or $l(t') \rightarrow l_M^-$. Then, from (17), it can be derived that

$$\begin{aligned} \lim_{t \rightarrow t'} \frac{k_l e_l^2}{\arctan(l - l_m) \arctan(l_M - l)} &= +\infty \\ \implies \lim_{t \rightarrow t'} V(t) &= +\infty, \end{aligned} \quad (21)$$

which is contradicted with (20). Hence, it follows from reduction to absurdity that the cable length is always limited within the given range, i.e.,

$$0 < l_m < l < l_M. \quad (22)$$

Then, the following conclusions can be obtained from (17) and (20):

$$\begin{aligned} e_{\theta_s}, \quad e_x, \quad e_l, \quad \dot{\theta}_s, \quad \dot{x}, \quad \dot{l}, \quad \dot{\theta}_1, \quad \dot{\theta}_2 &\in \mathcal{L}_\infty, \\ \theta_{sv}, \quad \dot{\theta}_{sv}, \quad x_v, \quad \dot{x}_v, \quad l_v, \quad \dot{l}_v &\in \mathcal{L}_\infty, \\ \tilde{m}_{cp} \in \mathcal{L}_\infty &\implies \hat{m}_{cp} \in \mathcal{L}_\infty. \end{aligned} \quad (23)$$

After that, in order to demonstrate that $\tau_s(t)$, $F_x(t)$, $F_l(t)$ in (10)–(12) are bounded, it remains to prove $\hat{m}_{cs} \in \mathcal{L}_\infty$ [see (14)]. It is obvious that $\frac{(\int_0^t e_l d\rho)^2}{1 + (\int_0^t e_l d\rho)^2} < 1$; then, together with $e_l \in \mathcal{L}_\infty$ from (23), it can be concluded that

$$\hat{m}_{cs} \in \mathcal{L}_\infty. \quad (24)$$

Hence, it can be derived from (10)–(12), (23), and (24), that

$$\tau_s, \quad F_x, \quad F_l \in \mathcal{L}_\infty \implies \ddot{\theta}_s, \quad \ddot{x}, \quad \ddot{l}, \quad \ddot{\theta}_1, \quad \ddot{\theta}_2 \in \mathcal{L}_\infty. \quad (25)$$

Step 2: The proof of the asymptotic stability will be further completed by introducing an invariant set. To this end, one can use Lemma 1 and first define a set \mathcal{S} as follows:

$$\mathcal{S} = \left\{ \theta_s, \quad x, \quad \theta_1, \quad \theta_2, \quad \dot{\theta}_s, \quad \dot{x}, \quad \dot{\theta}_1, \quad \dot{\theta}_2 \mid \dot{V} = 0 \right\}, \quad (26)$$

and define \mathcal{M} as the largest invariant set which is contained in \mathcal{S} . Hence, according to (18), in \mathcal{M} , it is valid that

$$\begin{aligned} \dot{\theta}_s &= 0, \quad \dot{x}_v = 0, \quad \dot{l}_v = 0 \implies \ddot{\theta}_s = 0, \quad \ddot{x}_v = 0, \quad \ddot{l}_v = 0, \\ \implies \theta_{sv} &= \alpha_1, \quad x_v = \alpha_2, \quad l_v = \alpha_3, \end{aligned} \quad (27)$$

where $\alpha_1, \alpha_2, \alpha_3 \in \mathbb{R}$ are constants. Also, for the introduced virtual system (5), we can derive that in \mathcal{M} ,

$$\begin{aligned} k_{v\theta_{s,1}} (\alpha_1 - \beta_1) &= k_{v\theta_{s,2}} (\theta_{sd} - \alpha_1), \\ k_{vx,1} (\alpha_2 - \beta_2) &= k_{vx,2} (x_d - \alpha_2), \\ k_{vl,1} (\alpha_3 - \beta_3) &= k_{vl,2} (l_d - \alpha_3), \end{aligned} \quad (28)$$

where $\beta_1, \beta_2, \beta_3 \in \mathbb{R}$ are constants with the following definitions:

$$\theta_s = \beta_1, \quad x = \beta_2, \quad l = \beta_3. \quad (29)$$

Then, by inserting (10)–(12) and (27)–(29) into (50)–(54), one has that

$$\begin{aligned} m_c \alpha_3^2 \cos \theta_2 \sin \theta_1 \sin \theta_2 \dot{\theta}_1^2 &+ 2m_c \alpha_3^2 \dot{\theta}_1 \dot{\theta}_2 \cos \theta_1 \sin^2 \theta_2 \\ - m_c \alpha_3 \alpha_2 \sin \theta_2 \cdot \dot{\theta}_2^2 &- m_c \alpha_3^2 \dot{\theta}_1 \cos \theta_2 \cos \theta_1 \sin \theta_2 + \ddot{\theta}_2 \\ \cdot (m_c \alpha_3^2 \sin \theta_1 + m_c \alpha_3 \alpha_2 \cos \theta_2) &= -k_1 (\alpha_1 - \theta_{sd}), \end{aligned} \quad (30)$$

$$\begin{aligned} -m_c \alpha_3 \cos \theta_2 \sin \theta_1 \cdot \dot{\theta}_1^2 &- 2m_c \alpha_3 \cos \theta_1 \sin \theta_2 \cdot \dot{\theta}_1 \dot{\theta}_2 \\ -m_c \alpha_3 \cos \theta_2 \sin \theta_1 \cdot \dot{\theta}_1^2 &- m_c \alpha_3 \sin \theta_1 \sin \theta_2 \cdot \ddot{\theta}_2 \\ + m_c \alpha_3 \cos \theta_2 \cos \theta_1 \cdot \ddot{\theta}_1 &= -k_2 (\alpha_2 - x_d), \end{aligned} \quad (31)$$

$$\begin{aligned} -m_c \alpha_3 \cos^2 \theta_1 \cdot \dot{\theta}_1^2 &- m_c \alpha_3 \dot{\theta}_2^2 + m_c g \cos \theta_1 \cos \theta_2 \\ = -k_3 (\alpha_3 - l_d) &- y(\alpha_3) + (\hat{m}_{cp} + \hat{m}_{cs}) g, \end{aligned} \quad (32)$$

$$\begin{aligned} -2m_c \alpha_3 \sin \theta_2 \cos \theta_2 \cdot \dot{\theta}_1 \dot{\theta}_2 &+ m_c \alpha_3 \cos^2 \theta_2 \cdot \ddot{\theta}_1 \\ + m_c g \cos \theta_2 \sin \theta_1 &= 0, \end{aligned} \quad (33)$$

$$\begin{aligned} m_c \alpha_3 \cos \theta_2 \sin \theta_2 \cdot \dot{\theta}_1^2 &+ m_c \alpha_3 \ddot{\theta}_2 \\ + m_c g \cos \theta_1 \sin \theta_2 &= 0, \end{aligned} \quad (34)$$

where $k_1 = k_{p1} (k_{v\theta_{s,1}} + k_{v\theta_{s,2}}) / k_{v\theta_{s,1}} + k_{v\theta_{s,2}}$, $k_2 = k_{p2} (k_{vx,1} + k_{vx,2}) / k_{vx,1} + k_{vx,2}$, $k_3 = k_{p3} (k_{vl,1} +$

$k_{vl,2})/k_{vl,1} + k_{vl,2}$. By integrating both sides of (30) and (31), they become

$$\begin{aligned} -m_c \alpha_3^2 \cos \theta_1 \cos \theta_2 \sin \theta_2 \cdot \dot{\theta}_1 + (m_c \alpha_3^2 \sin \theta_1 \\ + m_c \alpha_3 \alpha_1 \cos \theta_2) \dot{\theta}_2 = -k_1(\alpha_1 - \theta_{sd})t + \lambda_1, \end{aligned} \quad (35)$$

$$\begin{aligned} -m_c \alpha_3 \sin \theta_2 \sin \theta_1 \cdot \dot{\theta}_2 + m_c \alpha_3 \cos \theta_2 \cos \theta_1 \cdot \dot{\theta}_1 \\ = -k_2(\alpha_2 - x_d)t + \lambda_2, \end{aligned} \quad (36)$$

where $\lambda_1, \lambda_2 \in \mathbb{R}^+$ are constants. If $\alpha_1 - \theta_{sd} \neq 0$ ($\alpha_2 - x_d \neq 0$), then the left side of (35) [(36)] tends to infinity when $t \rightarrow +\infty$, which is contradicted with the conclusion in (23); hence, one can conclude that

$$\begin{aligned} \alpha_1 - \theta_{sd} = 0, \quad \alpha_2 - x_d = 0 \\ \Rightarrow \theta_s = \beta_1 = \alpha_1 = \theta_{sd}, \quad x = \beta_2 = \alpha_2 = x_d, \end{aligned} \quad (37)$$

where (28) and (29) are utilized. Then, by multiplying both sides of (31) by $\cos \theta_2/m_c$, the following equations can be obtained:

$$\begin{aligned} \alpha_3 \cos^2 \theta_2 \cos \theta_1 \cdot \ddot{\theta}_1 - \alpha_3 \sin \theta_2 \sin \theta_1 \cos \theta_2 \cdot \ddot{\theta}_2 \\ - \alpha_3 \cos^2 \theta_2 \sin \theta_1 \cdot \dot{\theta}_2^2 - 2\alpha_3 \cos \theta_1 \cos \theta_2 \sin \theta_2 \cdot \dot{\theta}_1 \dot{\theta}_2 \\ - \alpha_3 \cos^2 \theta_2 \sin \theta_1 \cdot \dot{\theta}_1^2 = 0, \end{aligned} \quad (38)$$

where (37) is utilized. Also, after dividing both sides of (33) and (34) by m_c , we may obtain, after mathematical arrangements, that

$$\begin{aligned} \alpha_3 \cos^2 \theta_2 \cdot \ddot{\theta}_1 = 2\alpha_3 \sin \theta_2 \cos \theta_2 \cdot \dot{\theta}_1 \dot{\theta}_2 - g \cos \theta_2 \sin \theta_1, \\ \alpha_3 \ddot{\theta}_2 = -\alpha_3 \cos \theta_2 \sin \theta_2 \cdot \dot{\theta}_1^2 - g \cos \theta_1 \sin \theta_2. \end{aligned} \quad (39)$$

After substituting (39) into (38), one has that

$$\begin{aligned} \sin \theta_1 \cos^2 \theta_2 \left(g \cos \theta_1 \cos \theta_2 + \alpha_3 \dot{\theta}_1^2 \cos^2 \theta_2 + \alpha_3 \dot{\theta}_2^2 \right) = 0, \\ \Rightarrow \sin \theta_1 = 0, \end{aligned} \quad (40)$$

where Assumption 1 and $\cos^2 \theta_2 + \sin^2 \theta_1 \equiv 1$ are employed. From (40), one can conclude that

$$\sin \theta_1 = 0 \Rightarrow \theta_1 = 0, \quad \dot{\theta}_1 = 0, \quad \ddot{\theta}_1 = 0. \quad (41)$$

Furthermore, by inserting (37) and (41), and integrating both sides of (35), the following equations can be obtained:

$$\begin{aligned} m_c \alpha_3 \alpha_1 \cos \theta_2 \cdot \dot{\theta}_2 = \lambda_1 \\ \Rightarrow m_c \alpha_3 \alpha_1 \sin \theta_2 = \lambda_1 t + \lambda_3, \end{aligned} \quad (42)$$

where $\lambda_3 \in \mathbb{R}^+$ is a constant. If $\lambda_1 \neq 0$, then in (42), it is implied that $\lim_{t \rightarrow +\infty} m_c \alpha_3 \alpha_1 \sin \theta_2 = +\infty$, which is contradicted with $m_c \alpha_3 \alpha_1 \sin \theta_2 \in \mathcal{L}_\infty$; hence,

$$\begin{aligned} \lambda_1 = 0 \Rightarrow \sin \theta_2 = \lambda_3, \\ \Rightarrow \dot{\theta}_2 = 0, \quad \ddot{\theta}_2 = 0. \end{aligned} \quad (43)$$

After inserting (41) and (43) into (34), one has that

$$m_c g \cos \theta_1 \sin \theta_2 = 0 \Rightarrow \theta_2 = 0. \quad (44)$$

In addition, according to the conclusions in (41), (43), and (44), equation (32) becomes

$$m_c g = -k_3(\alpha_3 - l_d) - y(\alpha_3) + (\hat{m}_{cp} + \hat{m}_{cs})g. \quad (45)$$

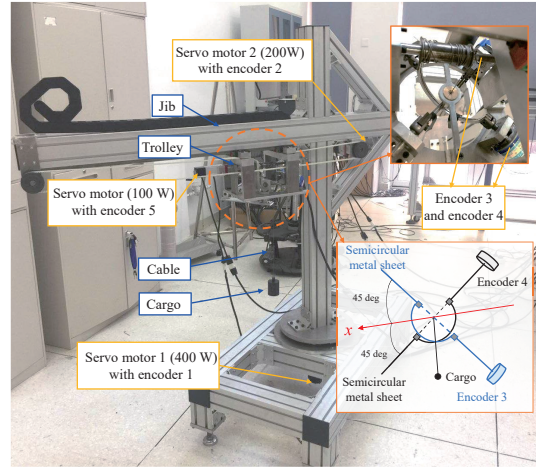


Fig. 4. The hardware platform of the varying-cable-length tower crane system.

As defined in (14), it is true that

$$k_{m2}(\alpha_3 - l_d)g \cdot \frac{(\alpha_3 - l_d)^2 t^2}{1 + (\alpha_3 - l_d)^2 t^2} = \gamma, \quad (46)$$

where $\gamma \triangleq m_c g + k_3(\alpha_3 - l_d) + y(\alpha_3) - \hat{m}_{cp}g$ is a constant. If $l - l_d = \alpha_3 - l_d \neq 0$, then (46) is invalid (the left side is time varying but the right side is constant); hence, from (28) and (29), one has that

$$\alpha_3 - l_d = 0 \Rightarrow l = \beta_3 = \alpha_3 = l_d, \quad (47)$$

by using (28). From (45) and (47), it can be obtained that

$$\hat{m}_c = \hat{m}_{cp} + \hat{m}_{cs} = m_c. \quad (48)$$

In sum, it can be concluded from (23), (27), (37), (41), (43), (44), (47), and (48) that, in \mathcal{M} ,

$$e_{\theta_s} = 0, \quad e_x = 0, \quad e_l = 0, \quad \theta_1 = 0, \quad \theta_2 = 0, \quad \tilde{m}_c = 0, \quad (49)$$

implying that \mathcal{M} only contains the closed-loop equilibrium point, and hence, by using LaSalle's Invariance Theorem given in Lemma 1, we can obtain that the error signals/swing angles asymptotically converge to zero, i.e.,

$$e_{\theta_s} \rightarrow 0, \quad e_x \rightarrow 0, \quad e_l \rightarrow 0, \quad \theta_1 \rightarrow 0, \quad \theta_2 \rightarrow 0, \quad \tilde{m}_c \rightarrow 0.$$

Then the proof of Theorem 1 is finished. ■

Remark 2: Under the present framework, it is difficult to theoretically analyze the robustness of the proposed controller (10)–(12) against external disturbances, which will be examined by hardware experiments in Section IV. Theoretically analyzing of the robustness against external disturbances will be treated as an important topic in our future studies.

IV. HARDWARE EXPERIMENTS

In this section, for verification, hardware experiments will be implemented on a self-built tower crane platform, as shown in Fig. 4. Specifically, the jib rotates around the mast and also serves as the “rail” for the trolley. In addition, to realize cargo hoisting/lowering, the suspension cable is wounded around a reel. The jib slew motion, the trolley translation, and the

TABLE II
MEASUREMENT PRECISIONS

Encoder/Motor	Variable	Measurement Precision
motor 1 with encoder 1 (2500 PPR)	$\theta_s(t)$	0.036 deg
motor 2 with encoder 2 (2500 PPR)	$x(t)$	0.013 mm
encoders 3&4 (2000 PPR)	$\theta_1(t), \theta_2(t)$	0.045 deg
motor 5 with encoder 5 (2500 PPR)	$l(t)$	0.006 mm

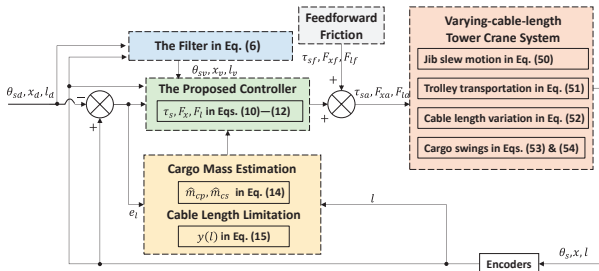


Fig. 5. The block diagram of the entire control system.

cargo hoisting/lowering motion are all actuated by AC servo motors equipped with encoders. With the help of the built-in encoders (encoders 1, 2, and 5), the jib slew angle, the trolley displacement, and the cable length can be measured. Also, the angular measurement structure is carefully designed by using two semicircular metal sheets, being vertically equipped on the trolley. Two independent encoders (encoders 3 and 4) are equipped to obtain the sheets' rotational angles so as to finally obtain the cargo swing angles based on the angular relationship. The measurement precisions are given in TABLE II. All measured signals are collected by a control board and are sent to a computer to generate real-time control signals by the MATLAB/Simulink Real Time Windows Target. The calculated control signals are then sent back to actuators through the control board.

The system parameters are set, for the platform, as follows:

$$m_t = 8 \text{ kg}, J = 6.8 \text{ kg} \cdot \text{m}^2, g = 9.8 \text{ m/s}^2,$$

and the sampling period is 5 ms. The frictions τ_{sf} , F_{xf} , F_{lf} are addressed through feedforward compensation. Inspired by the friction model in [33], the frictions are approximately determined as $\tau_{sf} = f_{\tau 1} \tanh(f_{\tau 2} \dot{\theta}_s) + f_{\tau 3} |\dot{\theta}_s| \dot{\theta}_s$, $F_{xf} = f_{x1} \tanh(f_{x2} \dot{x}) + f_{x3} |\dot{x}| \dot{x}$, $F_{lf} = f_{l1} \tanh(f_{l2} \dot{l}) + f_{l3} |\dot{l}| \dot{l}$. After abundant previous off-line experiments and data fitting, the friction coefficients are ultimately identified as $f_{\tau 1} = 34.11$, $f_{\tau 2} = 1$, $f_{\tau 3} = 0.329$, $f_{x1} = 35.77$, $f_{x2} = 8000.11$, $f_{x3} = 90$, $f_{l1} = 38$, $f_{l2} = 2000$, $f_{l3} = 88$, and the unavailable velocities are replaced by the dynamical signals $\dot{\theta}_{sv}(t)$, $\dot{x}_v(t)$, $\dot{l}_v(t)$ generated by (6).

Then, three groups of experiments are implemented.

Experiment 1: Comparative Experiments. In this group, the proposed controller and a linear quadratic regulator (LQR) controller are applied to transport the cargo from its initial position to the desired position. The initial/final conditions are set as $\theta_s(0) = 0$ deg, $x(0) = 0$ m, $l(0) = 0.3$ m, $\theta_{sd} = 45$ deg, $x_d = 0.5$ m, and $l_d = 0.5$ m. Also, $m_c = 1$ kg, $l_m = 0.01$ m, and $l_M = 1$ m.

For the proposed controller, the control gains/coefficients are set as $k_{p1} = 35$, $k_{p2} = 86$, $k_{p3} = 220$, $k_{m1} =$

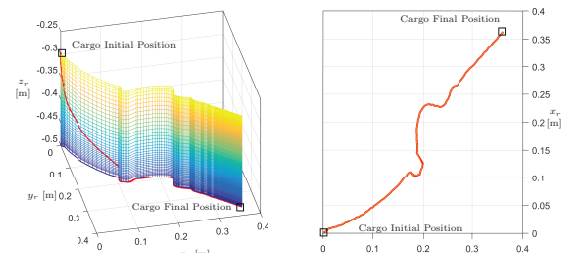


Fig. 6. 3D plot of the results of **Experiment 1** by applying the proposed controller (the red line—the cargo trajectory within $\{O - x_r y_r z_r\}$).

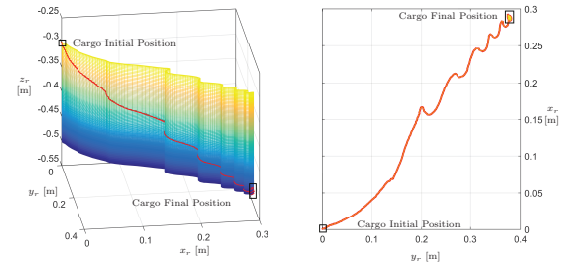


Fig. 7. 3D plot of the results of **Experiment 1** by applying the LQR controller (the red line—the cargo trajectory within $\{O - x_r y_r z_r\}$).

0.4, $k_{m2} = 0.15$, $k_l = 0.01$. Also, the parameters of the constructed virtual system (5) are given as $m_{v,\theta_s} = m_{v,x} = m_{v,l} = 1$, $\varphi_{\theta_s} = \varphi_x = \varphi_l = 0.1$, $k_{v\theta_s,1} = 12$, $k_{vx,1} = 1.6$, $k_{vl,1} = 2$, $k_{v\theta_s,2} = 5$, $k_{vx,2} = 0.5$, $k_{vl,3} = 0.5$, $i = 1, 2, 3$. As shown by the framework of the entire control system depicted in Fig. 5, the tuned control gains are applied to the proposed controller given in (10)–(12) to obtain the corresponding control inputs for the experiments. Specifically, as shown in Fig. 5, the measured real-time signals (through the encoders) and the tuned control gains are substituted together into the proposed controller given in (10)–(12) to calculate the control inputs during each control period.

For the LQR method, with the approximations of $\sin \theta_1 \approx \theta_1$, $\cos \theta_1 \approx 1$, $\sin \theta_2 \approx \theta_2$, $\cos \theta_2 \approx 1$, $\dot{\theta}_1^2 \approx 0$, $\dot{\theta}_2^2 \approx 0$, we first linearize the tower crane dynamics around the equilibrium point and obtain three decoupled linear systems [25], i.e., the slew subsystem, the translation subsystem, and the cable variation subsystem. By choosing $Q = \text{diag}\{10, 14, 150, 0\}$, $R = 0.01$ for the first two subsystems and $Q = \text{diag}\{10, 14\}$, $R = 0.01$ for the third subsystem, the LQR controller can be expressed as $\tau_s = -k_1 e_{\theta_s} - k_2 \dot{\theta}_s - k_3 \theta_2 - k_4 \dot{\theta}_2$, $F_x = -k_5 e_x - k_6 \dot{x} - k_7 \theta_1 - k_8 \dot{\theta}_1$, $F_l = -k_9 e_l - k_{10} \dot{l} - m_{cg}$, with the control gains k_i 's, $i = 1, 2, \dots, 10$, being calculated as $k_1 = 31.6$, $k_2 = 51.8$, $k_3 = -109.9$, $k_4 = -8.8$, $k_5 = 31.6$, $k_6 = 50.5$, $k_7 = -112.1$, $k_8 = -4.8$, $k_9 = -31.6$, $k_{10} = -38.3$, by applying the MATLAB Control System Toolbox.

The control gains of both controllers are obtained through carefully tuning, with the purpose of artificially unifying the maximum swing amplitudes to some extent, so that one can investigate the performance of other indicators, such as the response speed of positioning, residual swings, and position accuracy.

3-dimensional (3D) plots are provided for the comparative

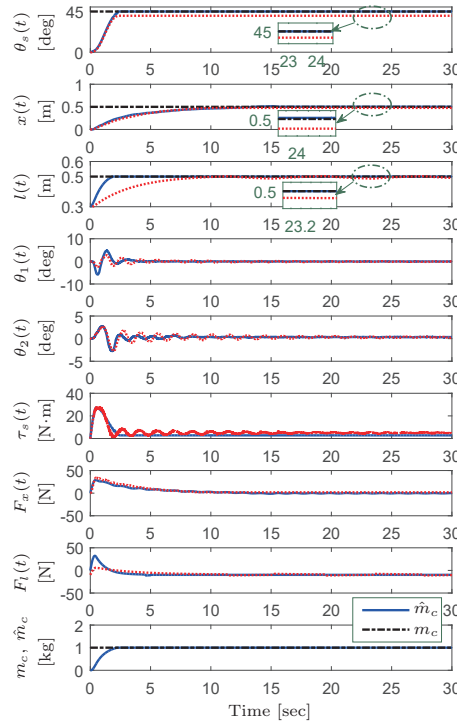


Fig. 8. Results of **Experiment 1** (the blue solid line—the proposed method; the red dashed line—the LQR controller).

results of **Experiment 1** in Figs. 6 and 7, to intuitively show the entire transportation process by drawing the cargo trajectories within the 3D workspace. The cargo trajectories are highlighted by red solid lines with square marks showing the cargo initial/final positions. It can be seen from the vertical views given in the right subplots of Figs. 6 and 7 that, compared with the LQR controller, the proposed method achieves more effective swing suppression, as the trajectory has fewer waves. Moreover, corresponding to Figs. 6 and 7, detailed comparative results are also given in Fig. 8. In Fig. 8, it can be seen from the subplots of $\theta_s(t)$, $x(t)$, and $l(t)$ that the LQR controller *fails* to eliminate the positioning errors while the proposed controller achieves accurate positioning; the subplot of $l(t)$ also shows that the proposed controller spends less time (about 2 s) than the LQR controller (after 8 s) to realize the same objective; in the subplots of $\theta_1(t)$ and $\theta_2(t)$, residual swings still exist after 30 s when applying the LQR controller, while by contrast, the swings are effectively eliminated at about 5 s when applying the proposed controller. Therefore, compared with the LQR controller, the proposed control method exhibits better control performance with much higher positioning accuracy and more effective swing suppression, and can also identify the exact value of the unknown cargo mass (corresponding to the last subplot of Fig. 8). It is worth mentioning that although the proposed controller only uses output feedback, it still achieves such satisfactory control performance in the presence of parametric uncertainties, which is one important merit.

Experiment 2: Unknown Cargo Mass Identification. Considering that accurate cargo masses are difficult to measure in practice, the adaptability of the proposed method to

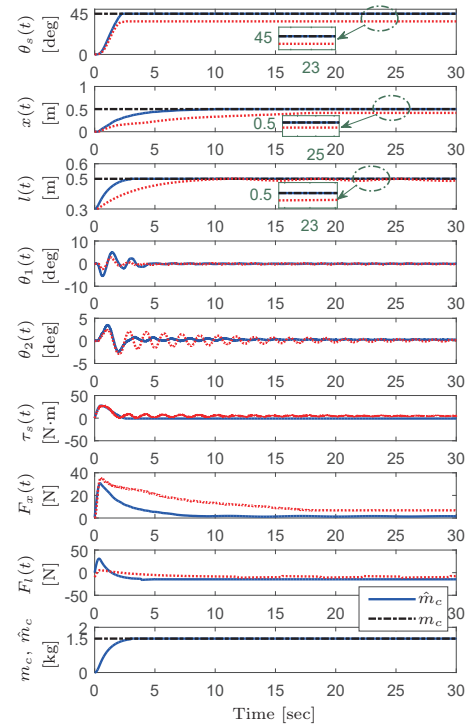


Fig. 9. Results of **Experiment 2** (the blue solid line—the proposed method; the red dashed line—the LQR controller).

unknown cargo mass is verified in this experiment. Here, compared with **Experiment 1**, the actual mass of the cargo is changed to $m_c = 1.5$ kg while the nominal mass remains 1 kg. The parameters, conditions, and the values of control gains/coefficients remain the *same*. The LQR controller is also applied for comparison.

The results of **Experiment 2** are shown in Fig. 9. It can be seen from Fig. 9 that, the changed cargo mass affects the control performance of the LQR controller with more obvious positioning errors and residual swings, while the proposed control method still achieves accurate positioning and effective swing damping. Moreover, the proposed controller can also recover the exact value of the unknown cargo mass accurately.

Experiment 3: Robustness Verification. This group further verifies the robustness of the proposed control method by considering the following two kinds of disturbances (the disturbances are all manually added by using a stick to knock the cargo):

- **Case 1: Non-Zero Initial Disturbances.** For the proposed controller, the initial values of the cargo swing angles $\theta_1(t)$ and $\theta_2(t)$ are set as $\theta_1(0) = 13.78$ deg and $\theta_2(0) = -16.99$ deg; for the comparative LQR method, the angles are $\theta_1(0) = 11.16$ deg and $\theta_2(0) = -10.22$ deg.
- **Case 2: External Disturbances.** The cargo swing angles $\theta_1(t)$ and $\theta_2(t)$ are disturbed during the control process at 8 s approximately.

The results of **Experiment 3** are shown in Figs. 10 and 11, which also include the results of the LQR controller for comparison. Specifically, in *Case 1*, it can be seen from Fig. 10 that the swing angles $\theta_1(t)$ and $\theta_2(t)$ are initialized with large angular values and the proposed control method still

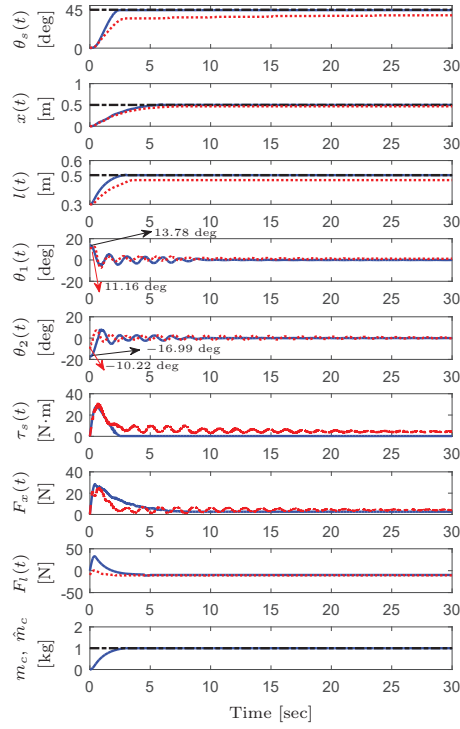


Fig. 10. Results of **Experiment 3: Case 1** (the *blue* solid line—the proposed method; the *red* dashed line—the LQR controller).

achieves satisfactory performance. Also, since tower cranes are usually applied in complex environments, in *Case 2*, additional disturbances are considered to testify the robustness. Correspondingly, in Fig. 11, the proposed control method effectively eliminates the influence induced by the external disturbances. For the LQR controller, as shown in Figs. 10 and 11, in both situations, after manually adding disturbances with similar amplitudes, the induced residual swings and positioning errors are obvious.

The results of **Experiments 1–3** indicate that the proposed control method exhibits satisfactory control performance with accurate positioning, effective swing elimination, and robustness against disturbances, which can also identify the exact values of cargo masses.

Remark 3: The control method can be executed by realizing the designed controller and adaptive law through programming languages. To this end, MATLAB is chosen as a software environment in this paper, which is replaceable. For practical applications, one can conveniently replace MATLAB, e.g., by C programming, and so on, as required.

Remark 4: Since the scale of the self-built tower crane hardware platform is small, the cargo swing amplitudes are not large (generally less than 10 deg) without manually adding disturbances. Hence, in this situation, the linearized model has little influence on the control performance of the LQR controller; since the small angle assumption is valid, it provides a fair comparison for the LQR controller and the proposed controller.

Remark 5: Since for crane systems, the cargo swing motion is, in fact, a reflection of the potential energy variation of the entire system, one can derive from the potential energy $P =$

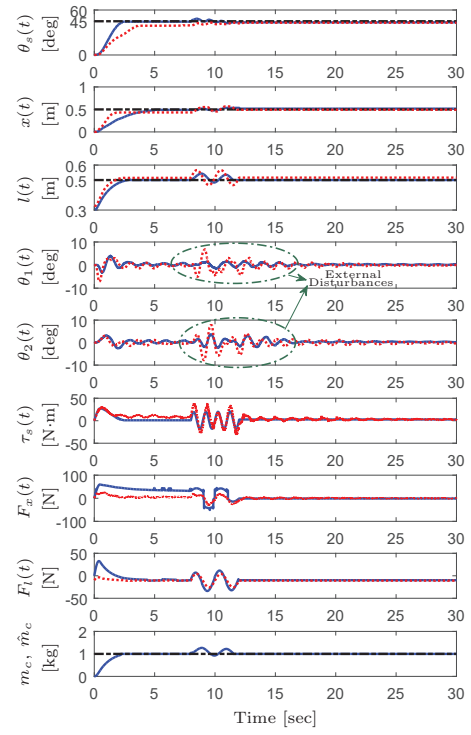


Fig. 11. Results of **Experiment 3: Case 2** (the *blue* solid line—the proposed method; the *red* dashed line—the LQR controller).

$m_{cg}l(1 - \cos \theta_1 \cos \theta_2)$ of the 5-DOF tower crane system that, for a given potential energy P , if the cable length $l(t)$ becomes larger, then the swing angles become relatively smaller. In this paper, the experimental results show that, in cases of the cable lengths not longer than 1 m, the proposed controller can achieve satisfactory performance with small swing amplitudes.

V. CONCLUSION

In this paper, an adaptive output feedback control method has been proposed for 5-DOF tower cranes, which is the *first* plant parameter-free output feedback approach designed/analyzed *without* linearizing dynamics that *simultaneously* achieves cargo transportation, swing suppression, mass identification, and cable length restriction with theoretical guarantee. Specifically, a virtual spring-masse system has been artificially introduced to avoid involving velocity signals. Also, through online identification, the exact values of unknown cargo masses can be estimated accurately. Asymptotically stable results are proven and moreover, groups of hardware experiments have been implemented by utilizing the self-built testbed. Experimental results are included to indicate the effectiveness of the proposed adaptive output feedback control approach. In future efforts, the output feedback control framework will be further improved by taking the frictions into consideration. Also, it will be another important future issue to investigate the disturbance-induced influence on the entire cable and the characteristics of the cable (e.g., flexibility, mass and density, etc.)

ACKNOWLEDGEMENT

The authors acknowledge the Associate Editor and all the reviewers for their great efforts in improving the manuscript.

APPENDIX A

EXPANDED EXPRESSIONS OF DYNAMIC EQUATIONS

Corresponding to (1), there are five expanded dynamic equations for the 5-DOF varying-cable-length tower crane system. Specifically, the dynamic equation of the actuated jib slew motion can be expressed as

$$\begin{aligned} & [J + (m_c + m_t)x^2 + m_c l^2 \sin^2 \theta_2 + m_c l^2 \cos^2 \theta_2 \sin^2 \theta_1 \\ & + 2m_c xl \cos \theta_2 \sin \theta_1] \ddot{\theta}_s - m_c l \ddot{x} \sin \theta_2 + m_c x l \ddot{l} \sin \theta_2 - m_c \\ & \cdot l^2 \dot{\theta}_1 \cos \theta_2 \cos \theta_1 \sin \theta_2 + (m_c l^2 \sin \theta_1 + m_c lx \cos \theta_2) \ddot{\theta}_2 \\ & + [2(m_c + m_t)x + 2m_c l \cos \theta_2 \sin \theta_1] \dot{x} \dot{\theta}_s + (2m_c l \sin^2 \theta_2 \\ & + 2m_c l \cos^2 \theta_2 \sin^2 \theta_1 + 2m_c x \cos \theta_2 \sin \theta_1) \dot{l} \dot{\theta}_s + (2m_c xl \\ & \cdot \cos \theta_2 \cos \theta_1 + 2m_c l^2 \cos^2 \theta_2 \sin \theta_1 \cos \theta_1) \dot{\theta}_s \dot{\theta}_1 + (2m_c l^2 \\ & \cdot \sin \theta_2 \cos \theta_2 \cos^2 \theta_1 - 2m_c xl \sin \theta_1 \sin \theta_2) \dot{\theta}_s \dot{\theta}_2 - 2m_c l \dot{l} \dot{\theta}_1 \\ & \cdot \cos \theta_1 \cos \theta_2 \sin \theta_2 + (2m_c l \sin \theta_1 + 2m_c x \cos \theta_2) \dot{l} \dot{\theta}_2 \\ & + m_c l^2 \dot{\theta}_1^2 \cos \theta_2 \sin \theta_1 \sin \theta_2 + 2m_c l^2 \dot{\theta}_1 \dot{\theta}_2 \cos \theta_1 \sin^2 \theta_2 \\ & - m_c lx \dot{\theta}_2^2 \sin \theta_2 = \tau_s. \end{aligned} \quad (50)$$

The dynamic equation of the actuated trolley translational motion is given as

$$\begin{aligned} & -m_c l \ddot{\theta}_s \sin \theta_2 + (m_c + m_t) \ddot{x} + m_c l \ddot{l} \cos \theta_2 \sin \theta_1 + m_c l \ddot{\theta}_1 \\ & \cdot \cos \theta_2 \cos \theta_1 - m_c l \dot{\theta}_2 \sin \theta_2 \sin \theta_1 - [m_c l \cos \theta_2 \sin \theta_1 \\ & + (m_c + m_t)x] \dot{\theta}_s^2 - 2m_c l \dot{\theta}_s \sin \theta_2 - 2m_c l \dot{\theta}_s \dot{\theta}_2 \cos \theta_2 \\ & + 2m_c l \dot{\theta}_1 \cos \theta_1 \cos \theta_2 - 2m_c l \dot{\theta}_2 \sin \theta_1 \sin \theta_2 \\ & - m_c l \dot{\theta}_1^2 \cos \theta_2 \sin \theta_1 - 2m_c l \dot{\theta}_1 \dot{\theta}_2 \cos \theta_1 \sin \theta_2 \\ & - m_c l \dot{\theta}_2^2 \cos \theta_2 \sin \theta_1 = F_x. \end{aligned} \quad (51)$$

Also, the dynamic equation corresponding to the cable length varying motion can be described as follows:

$$\begin{aligned} & m_c x \ddot{\theta}_s \sin \theta_2 + m_c \ddot{x} \cos \theta_2 \sin \theta_1 + m_c \ddot{l} - [m_c x \cos \theta_2 \sin \theta_1 \\ & + m_c l^2 \cos^2 \theta_2 \sin^2 \theta_1 + m_c l \sin^2 \theta_2] \dot{\theta}_s^2 + 2m_c \dot{\theta}_s \dot{x} \sin \theta_2 \\ & + 2m_c l \dot{\theta}_s \dot{\theta}_1 \cos \theta_2 \cos \theta_1 \sin \theta_2 - 2m_c l \dot{\theta}_s \dot{\theta}_2 \sin \theta_1 - m_c l \dot{\theta}_2^2 \\ & - m_c l \dot{\theta}_1^2 \cos^2 \theta_2 + m_c g \cos \theta_1 \cos \theta_2 = F_l. \end{aligned} \quad (52)$$

As for the unactuated cargo swing motion, the dynamic equations are provided in the following two equations for the radial and tangential swing directions, respectively:

$$\begin{aligned} & -m_c l^2 \ddot{\theta}_s \cos \theta_2 \cos \theta_1 \sin \theta_2 + m_c l \ddot{x} \cos \theta_2 \cos \theta_1 + m_c l^2 \ddot{\theta}_1 \\ & \cdot \cos^2 \theta_2 - (m_c l^2 \cos^2 \theta_2 \cos \theta_1 \sin \theta_1 + m_c lx \cos \theta_1 \cos \theta_2) \\ & \cdot \dot{\theta}_s^2 - 2m_c l \dot{l} \dot{\theta}_s \cos \theta_1 \sin \theta_2 \cos \theta_2 - 2m_c l^2 \dot{\theta}_s \dot{\theta}_2 \cos^2 \theta_2 \\ & \cdot \cos \theta_1 + 2m_c l \dot{l} \dot{\theta}_1 \cos^2 \theta_2 - 2m_c l^2 \dot{\theta}_1 \dot{\theta}_2 \sin \theta_2 \cos \theta_2 \\ & + m_c lg \cos \theta_2 \sin \theta_1 = 0, \end{aligned} \quad (53)$$

$$\begin{aligned} & (m_c l^2 \sin \theta_1 + m_c lx \cos \theta_2) \ddot{\theta}_s - m_c l \ddot{x} \sin \theta_2 \sin \theta_1 + m_c l^2 \\ & \cdot \ddot{\theta}_2 + (m_c lx \sin \theta_1 \sin \theta_2 - m_c l^2 \cos^2 \theta_1 \sin \theta_2 \cos \theta_2) \dot{\theta}_s^2 \\ & + 2m_c l \dot{x} \dot{\theta}_s \cos \theta_2 + 2m_c l \dot{l} \dot{\theta}_s \sin \theta_1 + 2m_c l^2 \dot{\theta}_s \dot{\theta}_1 \\ & \cdot \cos \theta_1 \cos^2 \theta_2 + m_c l^2 \dot{\theta}_1^2 \cos \theta_2 \sin \theta_2 \\ & + m_c lg \cos \theta_1 \sin \theta_2 = 0. \end{aligned} \quad (54)$$

APPENDIX B

DEFINITIONS OF $M(\mathbf{q})$, $C(\mathbf{q}, \dot{\mathbf{q}})$, $\mathbf{G}(\mathbf{q})$ IN (1)

The matrices $M(\mathbf{q})$, $C(\mathbf{q}, \dot{\mathbf{q}})$ and vector $\mathbf{G}(\mathbf{q})$ are specified as follows:

$$\begin{aligned} M(\mathbf{q}) &= \begin{bmatrix} m_{11}, & m_{12}, & m_{13}, & m_{14}, & m_{15} \\ m_{12}, & m_c + m_t, & m_{23}, & m_{24}, & m_{25} \\ m_{13}, & m_{23}, & m_c, & 0, & 0 \\ m_{14}, & m_{24}, & 0, & m_c l^2 \cos^2 \theta_2, & 0 \\ m_{15}, & m_{25}, & 0, & 0, & m_c l^2 \end{bmatrix}, \\ C(\mathbf{q}, \dot{\mathbf{q}}) &= \begin{bmatrix} c_{11}, & c_{12}, & c_{13}, & c_{14}, & c_{15} \\ c_{21}, & 0, & c_{23}, & c_{24}, & c_{25} \\ c_{31}, & c_{32}, & 0, & c_{34}, & c_{35} \\ c_{41}, & 0, & c_{43}, & c_{44}, & c_{45} \\ c_{51}, & c_{52}, & c_{53}, & c_{54}, & 0 \end{bmatrix}, \\ \mathbf{G}(\mathbf{q}) &= \begin{bmatrix} 0 \\ 0 \\ m_c g \cos \theta_1 \cos \theta_2 \\ m_c g l \cos \theta_2 \sin \theta_1 \\ m_c g l \cos \theta_1 \sin \theta_2 \end{bmatrix}. \end{aligned}$$

where

$$\begin{aligned} m_{11} &= J + (m_c + m_t)x^2 + m_c l^2 \sin^2 \theta_2 + m_c l^2 \cos^2 \theta_2 \sin^2 \theta_1 \\ & + 2m_c xl \cos \theta_2 \sin \theta_1, \\ m_{12} &= -m_c l \sin \theta_2, \quad m_{13} = m_c x \sin \theta_2, \\ m_{14} &= -m_c l^2 \cos \theta_2 \sin \theta_2 \cos \theta_1, \\ m_{23} &= m_c l \cos \theta_2 \sin \theta_1, \quad m_{24} = m_c l \cos \theta_2 \cos \theta_1, \\ m_{25} &= -m_c l \sin \theta_2 \sin \theta_1, \end{aligned}$$

and

$$\begin{aligned} c_{11} &= (m_c + m_t)x \dot{x} + m_c l(x \dot{\theta}_1 \cos \theta_1 \cos \theta_2 - x \dot{\theta}_2 \sin \theta_2 \sin \theta_1 \\ & + \dot{x} \sin \theta_1 \cos \theta_2) + m_c l^2(\dot{\theta}_1 \sin \theta_1 \cos \theta_1 \cos^2 \theta_2 \\ & + \dot{\theta}_2 \cos^2 \theta_1 \sin \theta_2 \cos \theta_2), \\ c_{12} &= [(m_c + m_t)x + m_c l \sin \theta_1 \cos \theta_1] \dot{\theta}_s + m_c l \dot{l} (\sin^2 \theta_2 \\ & + \cos^2 \theta_2 \sin^2 \theta_1) + m_c x \dot{l} \cos \theta_2 \sin \theta_1, \\ c_{13} &= m_c l \dot{\theta}_s (\sin^2 \theta_2 + \cos^2 \theta_2 \sin^2 \theta_1) + m_c x \dot{\theta}_s \cos \theta_2 \sin \theta_1, \\ c_{13} &= m_c l \dot{\theta}_s (\sin^2 \theta_2 + \cos^2 \theta_2 \sin^2 \theta_1) + m_c x \dot{\theta}_s \cos \theta_2 \sin \theta_1, \\ c_{14} &= m_c l x \dot{\theta}_s \cos \theta_1 \cos \theta_2 + m_c l^2(\dot{\theta}_s \sin \theta_1 \cos \theta_1 \cos^2 \theta_2 \\ & + \dot{\theta}_1 \sin \theta_1 \sin \theta_2 \cos \theta_2), \\ c_{15} &= -m_c l(x \dot{\theta}_s \sin \theta_2 \sin \theta_1 + x \dot{\theta}_2 \sin \theta_2) + m_c l^2(\dot{\theta}_s \cos^2 \theta_1 \\ & \times \sin \theta_2 \cos \theta_2 + \dot{\theta}_1 \cos \theta_1 \sin^2 \theta_2), \end{aligned}$$

$$\begin{aligned}
 c_{21} &= -(m_c + m_t)x\dot{\theta}_s - m_c l(\dot{\theta}_s \cos \theta_2 \sin \theta_1 \\
 &\quad + \dot{\theta}_2 \cos \theta_2) - m_c l \sin \theta_2, \\
 c_{23} &= -m_c \dot{\theta}_s \sin \theta_2 + m_c \dot{\theta}_1 \cos \theta_1 \cos \theta_2 - m_c \dot{\theta}_2 \sin \theta_1 \sin \theta_2, \\
 c_{24} &= -m_c l(\dot{\theta}_2 \cos \theta_1 \sin \theta_2 + \dot{\theta}_1 \cos \theta_2 \sin \theta_1) \\
 &\quad + m_c l \cos \theta_1 \cos \theta_2, \\
 c_{25} &= -m_c l(\dot{\theta}_1 \cos \theta_1 \sin \theta_2 + \dot{\theta}_2 \cos \theta_2 \sin \theta_1 + \dot{\theta}_s \cos \theta_2) \\
 &\quad - m_c l \sin \theta_1 \sin \theta_2, \\
 c_{31} &= [m_c x \cos \theta_2 \sin \theta_1 + m_c l^2 \cos^2 \theta_2 \sin^2 \theta_1 + m_c l \sin^2 \theta_2] \dot{\theta}_s \\
 &\quad + m_c \dot{x} \sin \theta_2 + m_c l \dot{\theta}_1 \cos \theta_2 \cos \theta_1 \sin \theta_2 - m_c l \dot{\theta}_2 \sin \theta_1, \\
 c_{32} &= m_c \dot{\theta}_1 \sin \theta_2, \\
 c_{34} &= -m_c l \dot{\theta}_1 \cos^2 \theta_2 + m_c l \dot{\theta}_s \cos \theta_2 \cos \theta_1 \sin \theta_2, \\
 c_{35} &= -m_c l \dot{\theta}_2 - m_c l \dot{\theta}_s \sin \theta_1, \\
 c_{41} &= -m_c l(x + l \sin \theta_1 \cos \theta_2) \dot{\theta}_s \cos \theta_1 \cos \theta_2 \\
 &\quad - m_c l^2 \dot{\theta}_2 \cos^2 \theta_2 \cos \theta_1 - m_c l \dot{l} \cos \theta_1 \sin \theta_2 \cos \theta_2, \\
 c_{43} &= -m_c l \dot{\theta}_s \cos \theta_1 \sin \theta_2 \cos \theta_2 + m_c l \dot{\theta}_1 \cos^2 \theta_2, \\
 c_{44} &= -m_c l^2 \dot{\theta}_2 \cos \theta_s \sin \theta_2 + m_c l \dot{l} \cos^2 \theta_2, \\
 c_{45} &= -m_c l^2(\dot{\theta}_s \cos \theta_1 \cos^2 \theta_2 + \dot{\theta}_1 \cos \theta_2 \sin \theta_2), \\
 c_{51} &= m_c l(\dot{x} \cos \theta_2 + x \dot{\theta}_s \sin \theta_1 \sin \theta_2 - l \dot{\theta}_s \cos^2 \theta_1 \sin \theta_2 \cos \theta_2) \\
 &\quad + m_c l^2 \dot{\theta}_1 \cos \theta_1 \cos^2 \theta_2 + m_c l \dot{l} \sin \theta_1, \\
 c_{52} &= m_c l \dot{\theta}_s \cos \theta_2, \quad c_{53} = m_c l \dot{\theta}_s \sin \theta_1, \\
 c_{54} &= m_c l^2(\dot{\theta}_s \cos \theta_1 \cos^2 \theta_2 + \dot{\theta}_1 \sin \theta_1 \cos \theta_2).
 \end{aligned}$$

APPENDIX C PROOF FOR POSITIVE DEFINITENESS OF $V(t)$

It will be proven that $V(t)$ shown in (17) is positive definite on $l(t) > 0$. First, we need to analyze the second, the seventh, and eighth terms of (17), since the other terms of $V(t)$ are obviously nonnegative. Using (22), it follows from (17) that

$$\begin{aligned}
 m_c g l(1 - \cos \theta_1 \cos \theta_2) &\geq 0, \\
 \frac{k_l e_l^2}{\arctan(l - l_m) \arctan(l_M - l)} &\geq 0.
 \end{aligned}$$

In addition, for convenience, the seventh term of (17) is defined as $\Delta(e_l) \triangleq g \int_0^{e_l} \hat{m}_{cs}(\tau) d\tau$. If $e_l = 0$, it holds that $\Delta(0) = 0$. If $e_l > 0$, it can be derived, by using (14), that $\frac{\partial \Delta}{\partial e_l} = \hat{m}_{cs}(e_l)g > 0$. Also, if $e_l < 0$, one has that $\frac{\partial \Delta}{\partial e_l} < 0$. The above analysis indicates that $\Delta(e_l)$ is increasing when $e_l > 0$ (decreasing when $e_l \leq 0$), leading to $\Delta = g \int_0^{e_l} \hat{m}_{cs}(\tau) d\tau \geq 0$.

Therefore, the second, the seventh, and the eighth terms are all nonnegative, and one can conclude that $V(t) \geq 0$. Also, $V(t) = 0$ holds if and only if state variables are at the equilibrium point, implying that $V(t)$ is positive definite.

REFERENCES

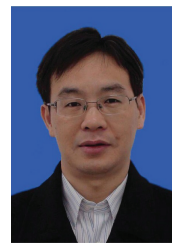
- [1] J. Yang, J. Su, S. Li, and X. Yu, "High-order mismatched disturbance compensation for motion control systems via a continuous dynamic sliding-mode approach," *IEEE Transactions on Industrial Informatics*, vol. 10, no. 1, pp. 604–614, 2014.
- [2] C. Yang, Y. Jiang, Z. Li, W. He, and C.-Y. Su, "Neural control of bimanual robots with guaranteed global stability and motion precision," *IEEE Transactions on Industrial Informatics*, vol. 13, no. 3, pp. 1162–1171, 2017.
- [3] W. Sun, S. Su, J. Xia, and Y. Wu, "Adaptive tracking control of wheeled inverted pendulums with periodic disturbances," *IEEE Transactions on Cybernetics*, in press, DOI: 10.1109/TCYB.2018.2884707.
- [4] X.-Z. Lai, J.-H. She, S. X. Yang, and M. Wu, "Comprehensive unified control strategy for underactuated two-link manipulators," *IEEE Transactions on Systems, Man, and Cybernetics, Part B—Cybernetics*, vol. 39, no. 2, pp. 389–398, 2009.
- [5] B. Xiao and S. Yin, "Exponential tracking control of robotic manipulators with uncertain dynamics and kinematics," *IEEE Transactions on Industrial Informatics*, vol. 15, no. 2, pp. 689–698, 2019.
- [6] H. Li, S. Zhao, W. He, and R. Lu, "Adaptive finite-time tracking control of full states constrained nonlinear systems with dead-zone," *Automatica*, vol. 100, pp. 99–107, 2019.
- [7] W. K. Ho, T. Chen, K. V. Ling, and L. Sun, "Variance analysis of robust state estimation in power system using influence function," *International Journal of Electrical Power & Energy Systems*, vol. 92, pp. 53–62, 2017.
- [8] Z. N. Masoud and K. A. Alhazza, "Frequency-modulation input shaping control of double-pendulum overhead cranes," *Journal of Dynamic Systems, Measurement, and Control*, vol. 136, no. 2, pp. 021005–1–11, 2014.
- [9] G. Boschetti, R. Caracciolo, D. Richiedei, and A. Trevisani, "Moving the suspended load of an overhead crane along a pre-specified path: A non-time based approach," *Robotics and Computer-Integrated Manufacturing*, vol. 30, no. 3, pp. 256–264, 2014.
- [10] P. Cai, I. Chandrasekaran, J. Zheng, and Y. Cai, "Automatic path planning for dual-crane lifting in complex environments using a prioritized multiobjective PGA," *IEEE Transactions on Industrial Informatics*, vol. 14, no. 3, pp. 829–845, 2018.
- [11] O. Sawodny, H. Aschemann, and S. Lahres, "An automated gantry crane as a large workspace robot," *Control Engineering Practice*, vol. 10, no. 12, pp. 1323–1338, 2002.
- [12] Q. H. Ngo and K. S. Hong, "Sliding-mode antisway control of an offshore container crane," *IEEE/ASME Transactions on Mechatronics*, vol. 17, no. 2, pp. 201–209, 2012.
- [13] C.-C. Tsai, H. L. Wu, and K.-H. Chuang, "Backstepping aggregated sliding-mode motion control for automatic 3D overhead cranes," in *Proceedings of the IEEE/ASME International Conference on Advanced Intelligent Mechatronics*, Kachsiung, Taiwan, 2012, pp. 849–854.
- [14] C.-Y. Chang, "Adaptive fuzzy controller of the overhead cranes with nonlinear disturbance," *IEEE Transactions on Industrial Informatics*, vol. 3, no. 2, pp. 164–172, 2007.
- [15] M. I. Solihin, Wahyudi, and A. Legowo, "Fuzzy-tuned PID anti-swing control of automatic gantry crane," *Journal of Vibration and Control*, vol. 16, no. 1, pp. 127–145, 2010.
- [16] D. Qian, S. Tong, and S.-G. Lee, "Fuzzy-logic-based control of payloads subjected to double-pendulum motion in overhead cranes," *Automation in Construction*, vol. 65, pp. 133–143, 2016.
- [17] J. Smoczek, "Fuzzy crane control with sensorless payload deflection feedback for vibration reduction," *Mechanical Systems and Signal Processing*, vol. 46, no. 1, pp. 70–81, 2014.
- [18] D. Wang, H. He, and D. Liu, "Intelligent optimal control with critic learning for a nonlinear overhead crane system," *IEEE Transactions on Industrial Informatics*, vol. 14, no. 7, pp. 2932–2940, 2018.
- [19] T. Kurabayashi and T. Murakami, "Position convergence and sway suppress method of overhead crane by emulating natural damping," in *Proceedings of the IEEE International Workshop on Advanced Motion Control*, Yokohama, Japan, 2014, pp. 610–615.
- [20] H. Park, D. Chwa, and K.-S. Hong, "A feedback linearization control of container cranes: Varying rope length," *International Journal of Control Automation and Systems*, vol. 5, no. 4, pp. 379–387, 2007.
- [21] G. Rigatos, P. Siano, and M. Abbaszadeh, "Nonlinear H-infinity control for 4-DOF underactuated overhead cranes," *Transactions of the Institute of Measurement and Control*, vol. 40, no. 7, pp. 2364–2377, 2018.
- [22] T. D. Ho and K. Terashima, "Robust control designs of payloads skew rotation in a boom crane system," *IEEE Transactions on Control Systems Technology*, vol. 27, no. 4, pp. 1608–1621, 2019.
- [23] J. Huang, X. Xie, and Z. Liang, "Control of bridge cranes with distributed-mass payload dynamics," *IEEE/ASME Transactions on Mechatronics*, vol. 20, no. 1, pp. 481–486, 2015.
- [24] L. Ramli, Z. Mohamed, A. M. Abdullahi, H. I. Jaafar, and I. M. Lazim, "Control strategies for crane systems: A comprehensive review," *Mechanical Systems and Signal Processing*, vol. 95, pp. 1–23, 2017.
- [25] D. Blackburn, J. Lawrence, J. Danielson, W. Singhose, T. Kamoi, and A. Taura, "Radial-motion assisted command shapers for nonlinear tower crane rotational slewing," *Control Engineering Practice*, vol. 18, no. 5, pp. 523–531, 2010.

- [26] M. Böck and A. Kugi, "Real-time nonlinear model predictive path-following control of a laboratory tower crane," *IEEE Transactions on Control Systems Technology*, vol. 22, no. 4, pp. 1461–1473, 2014.
- [27] H. M. Omar and A. H. Nayfeh, "Gain scheduling feedback control for tower cranes," *Journal of Vibration and Control*, vol. 9, no. 3–4 pp. 399–418, 2003.
- [28] W. Devesse, M. Ramteen, L. Feng, and J. Wikander, "A real-time optimal control method for swing-free tower crane motions," in *Proceedings of IEEE International Conference on Automation Science and Engineering*, Madison, WI, USA, 2013, pp. 336–341.
- [29] L. A. Tuan and S.-G. Lee, "3D cooperative control of tower cranes using robust adaptive techniques," *Journal of the Franklin Institute*, vol. 354, no. 18, pp. 8333–8357, 2017.
- [30] S. C. Duong, E. Uezato, H. Kinjo, and T. Yamamoto, "A hybrid evolutionary algorithm for recurrent neural network control of a three-dimensional tower crane," *Automation in Construction*, vol. 23, pp. 55–63, 2012.
- [31] I. G. Carmona and J. Collado, "Control of a two wired hammerhead tower crane," *Nonlinear Dynamics*, vol. 84, no. 4, pp. 2137–2148, 2016.
- [32] H. K. Khalil, *Nonlinear Systems*, 3rd ed. Englewood Cliffs, NJ: Prentice Hall, 2002.
- [33] C. Makkar, G. Hu, W. G. Sawyer, and W. E. Dixon, "Lyapunov-based tracking control in the presence of uncertain nonlinear parameterizable friction," *IEEE Transactions on Automatic Control*, vol. 52, no. 10, pp. 1988–1994, 2007.



He Chen received the B.S. degree in automation and the Ph. D. degree in control science and engineering from Nankai University, Tianjin, China, in 2013 and 2018, respectively. He is currently a Lecturer with the School of Artificial Intelligence, Hebei University of Technology, Tianjin, China.

His research interests include control of mechatronics, overhead cranes, and wheeled mobile robots.



Yongchun Fang (S'00–M'02–SM'08) received the B.S. degree and the M.S. degree in control theory and applications from Zhejiang University, Hangzhou, China, in 1996 and 1999, respectively, and the Ph.D. degree in electrical engineering from Clemson University, Clemson, SC, in 2002.

From 2002 to 2003, he was a Postdoctoral Fellow with the Sibley School of Mechanical and Aerospace Engineering, Cornell University, Ithaca, NY. He is currently a Professor with the Institute of Robotics and Automatic Information Systems, Nankai University, Tianjin, China. His research interests include nonlinear control, visual servoing, control of underactuated systems, and AFM-based nano-systems.



Yiming Wu received the B.S. degree in intelligent science and technology from Nankai University, Tianjin, China, in 2016. She is currently working towards the Ph.D. degree in control science and engineering, under the supervision of Dr. Ning Sun, with the Institute of Robotics and Automatic Information Systems, Nankai University, Tianjin, China.

Her research interests include the control of underactuated systems.



Ning Sun (S'12–M'14–SM'19) received the B.S. degree in measurement & control technology and instruments (with honors) from Wuhan University, Wuhan, China, in 2009, and the Ph.D. degree in control theory and control engineering (with honors) from Nankai University, Tianjin, China, in 2014.

He is currently an Associate Professor with the Institute of Robotics and Automatic Information Systems, Nankai University, Tianjin, China. He was awarded the prestigious Japan Society for the Promotion of Science (JSPS) Postdoctoral Fellowship

for Research in Japan (Standard) in 2018. His research interests include intelligent control for mechatronic/robotic systems with emphasis on (industrial) applications.

Dr. Sun received the Wu Wenjun Artificial Intelligence Excellent Youth Award in 2019, the China 10 Scientific and Technological Developments in Intelligent Manufacturing (2nd achiever) in 2019, the First Class Prize of Wu Wenjun Artificial Intelligence Natural Science Award in 2017, the First Class Prize of Tianjin Natural Science Award in 2018, the Golden Patent Award of Tianjin in 2017, the IJCAS (International Journal of Control, Automation, and Systems) Academic Activity Award in 2018, the Outstanding Ph.D. Dissertation Award from the Chinese Association of Automation (CAA) in 2016, etc. He is the Executive Editor for *Measurement and Control* and serves as an Associate Editor (editorial board member) for several journals, including *IEEE ACCESS*, *Frontiers in Neurorobotics*, *International Journal of Control, Automation, and Systems*, *IET Cyber-Systems & Robotics*, *Transactions of the Institute of Measurement and Control*, *International Journal of Precision Engineering and Manufacturing*, etc. Dr. Sun has been an Associate Editor of the IEEE Control Systems Society (CSS) Conference Editorial Board since July 2019.